ENGINEERING

Hydrophobic nanostructured wood membrane for thermally efficient distillation

Dianxun Hou[1], Tian Li[2], Xi Chen[1,3], Shuaiming He[2], Jiaqi Dai[2], Sohrab A. Mofid[4,5], Deyin Hou[6], Arpita Iddya[7], David Jassby[7], Ronggui Yang[4], Liangbing Hu[2]*, Zhiyong Jason Ren[1,3]*

Current membrane distillation (MD) is challenged by the inefficiency of water thermal separation from dissolved solutes, controlled by membrane porosity and thermal conductivity. Existing petroleum-derived polymeric membranes face major development barriers. Here, we demonstrate a first robust MD membrane directly fabricated from sustainable wood material. The hydrophobic nanowood membrane had high porosity (89 ± 3%) and hierarchical pore structure with a wide pore size distribution of crystalline cellulose nanofibrils and xylem vessels and lumina (channels) that facilitate water vapor transportation. The thermal conductivity was extremely low in the transverse direction, which reduces conductive heat transport. However, high thermal conductivity along the fiber enables efficient thermal dissipation along the axial direction. As a result, the membrane demonstrated excellent intrinsic vapor permeability (1.44 ± 0.09 kg m^{-1} K^{-1} s^{-1} Pa^{-1}) and thermal efficiency (~70% at 60°C). The properties of thermal efficiency, water flux, scalability, and sustainability make nanowood highly desirable for MD applications.

INTRODUCTION

Water scarcity is a worldwide grand challenge. The United Nations reported this year that nearly half of the global population (~3.6 billion) are currently living in potential water-scarce regions at least 1 month per year. This number could increase to between 4.8-5.7 billion by 2050 (*1*). This problem is exacerbated by climate change and rapid urbanization, evidenced by extensive periods of drought and more frequent wildfires in California and other regions (*2–4*). Desalination can help alleviate water stress by extracting fresh water from a range of saline or contaminated sources including seawater, brackish groundwater, or wastewater (*5, 6*), and the development of desalination has been greatly boosted by nanotechnology and advanced manufacturing (*7, 8*). However, although reaching its energy efficiency limit (~50%), current water desalination processes such as reverse osmosis are still energy intensive [2 to 4 kilowatt-hour m^{-3}] (*9, 10*). However, in many regions that can benefit from the technology, an increasing supply of renewable yet intermittent solar energy in the format of heat or electricity generates great opportunities for solar desalination, which also mitigate challenges in energy storage. By taking advantage of this low-cost and sometimes excess supply of heat or electrical energy, water desalination can become more cost effective (*11–13*).

Membrane distillation (MD) is an emerging thermally driven separation process with great potential for high-salinity water desalination using solar, thermal or other renewable sources (*10*). Driven by difference in temperature and vapor pressure. Water evaporates at the hot feed side of MD cells and diffuses through a porous hydrophobic membrane before condensing at the cold permeate side (*14–16*).

MD can be operated using low-grade heat such as condenser cooling water from thermal power plants or, increasingly, from renewable sources such as solar thermal or geothermal plants (*17–19*). During MD, the transport of water vapor leads to the convective heat transfer, where the heat partially conducts through the membrane materials thereby reducing temperature gradient and lowering the driving force for mass transfer across the membrane (*20, 21*). Thermal efficiency is an important parameter in MD and is defined as the convective heat flux across the membrane divided by the total heat flux (*22*). Accordingly, an ideal MD membrane would have a desired combination of characteristics, such as large pore size, low pore tortuosity, low thermal conductivity, high porosity, optimized thickness, good mechanical strength, cost competitiveness, and low environmental impacts (*10, 22–24*).

Current commercial MD membranes are made of synthetic polymers such as polytetrafluoroethylene (PTFE), polyvinylidene fluoride (PVDF), and polypropylene (PP) (*16, 25–27*). In general, these membranes have porosities lower than 0.80, thermal conductivities higher than 0.050 W m^{-1} K^{-1}, and thermal efficiency up to 60% (*10, 15, 16, 22, 25, 28*). For example, the microporous PTFE membranes are widely used in MD modules owing to their high hydrophobicity and stability (*26*), but many of these membranes are typically isotropic (fig. S4) and not ideal for highly effective thermal insulation (*29–31*). In addition, these polymer materials are derived from petroleum products, and their use and disposal generate environmental concerns due to low biodegradability (*32*). Therefore, MD membranes made from natural and low-cost materials with high thermal stability and hydrophobicity are highly desired, yet not available. Recently, Leitch *et al.* (*24*) presented a new bacterial nanocellulose aerogel MD membrane with high porosity (>98%) and low thermal conductivity (<0.03 W m^{-1} K^{-1}), demonstrating how membranes could be fabricated using natural materials.

In this study, we developed the first robust MD membrane directly from a sustainable wood material. Nanocellulose is an earth-abundant and, oftentimes, waste biomass source that has been used in products with minimal environmental and health impacts such as construction materials, body armor, biofuels, or water filters (*33–39*). Most nanocellulose-based products, such as paper (fig. S4), are from wood

[1]Department of Civil, Environmental, and Architectural Engineering, University of Colorado Boulder, Boulder, CO 80303, USA. [2]Department of Materials Science and Engineering, University of Maryland, College Park, MD 20742, USA. [3]Department of Civil and Environmental Engineering, Princeton University, Princeton, NJ 08544, USA. [4]Department of Mechanical Engineering, University of Colorado Boulder, Boulder, CO 80309, USA. [5]Department of Civil and Environmental Engineering, Norwegian University of Science and Technology, NO-7491 Trondheim, Norway. [6]State Key Laboratory of Environmental Aquatic Chemistry, Research Center for Eco-Environmental Sciences, Chinese Academy of Sciences, Beijing 100085, China. [7]Department of Civil and Environmental Engineering, University of California, Los Angeles, Los Angeles, CA 90095, USA.
*Corresponding author. Email: binghu@umd.edu (L.H.); zjren@princeton.edu (Z.J.R.)

pulp, where degraded cellulose fibers are randomly mixed together to form an isotropic structure with high density (1.20 g cm^{-3}) and lower mechanical strength (0.25 to 0.30 MPa) (40, 41). In contrast, this new wood membrane was made by directly removing lignin and semicellulose via chemical treatment and freeze-drying, which allowed the preservation of the anisotropic microstructure and hierarchical alignment of wood fibers. As a result, the wood can be prepared into an anisotropic and thermally insulating bulk material with extremely high porosity (~90%), low thermal conductivity (~0.04 W m^{-1} K^{-1}), and good mechanical strength (18 MPa), making it an ideal substrate for MD membrane. In this study, we report a nanostructured wood (i.e., nanowood) from natural American basswood followed by silane coating, which resulted in a hydrophobic nanowood membrane with high porosity yet very low thermal conductivity. The highly porous structure with naturally formed pores either amid the nanofibrils or growing on the wood vessels and fibril tracheid lumens (pits) reduces the water vapor transfer resistance and provides good water flux (20.8 ± 0.8 kg m^{-2} hour^{-1} at 60°C) in direct contact MD (DCMD) tests (Fig. 1). The anisotropic property can allow heat to spread along the nanofibril direction and reduce the conductive heat transfer, while the high intrinsic permeability enhances water vapor transfer and, thus, convective heat transfer. Together, these grant the membrane excellent thermal efficiency (71 ± 2% at 60°C) with one of the highest values among all the reported MD membranes in literature (22). The hydrophobic wood membranes were also compared with commercial membranes in terms of membrane structures [e.g., pore size distribution (PSD) and thermal conductivity] and MD performance (i.e., flux, vapor permeability, and thermal efficiency). Figure 1B shows a large piece of the nanowood membrane with a length of 18 cm, which demonstrates the scalability of the wood membrane fabrication process. To the best of our knowledge, this is the first report on a hydrophobic MD membrane made from a sustainable wood material.

RESULTS AND DISCUSSION
The unique porous structure of the hydrophobic nanostructure wood as a highly efficient membrane

The hydrophobic wood membranes (Fig. 2, A, B and C and Fig. 3, A and B) were directly derived from natural American basswood, in which amorphous lignin and hemicellulose are intertwined with cellulose nanofibrils (42). After chemical treatment and purification, as described in Materials and Methods, we preserved the wood microstructure and the hierarchical alignment. For the nanowood membrane, lignin and hemicellulose were removed, while the naturally aligned cellulose nanofibrils isolated from each other along the growth direction can be directly observed with the aid of scanning electron microscopy (SEM) (Fig. 2, D to H). The removal of intermixed lignin and hemicellulose for the nanowood membrane greatly reduced the linkage and interaction among cellulose fibrils and the fibril aggregates within the fibril wall, which greatly increased flexibility and porosity (39). The resulting aligned crystalline cellulose nanofibrils were held together by intermolecular hydrogen bonds and van der Waals forces (43). Presumably, this aligned structure with weakened interactions would reduce the thermal conductivity in the transverse direction, thereby mitigating the heat loss via the conductive heat transfer during MD.

Different from commercial membranes with vertical pores (e.g., finger-like structure; fig. S7) (26), the wood membranes presented a unique pore structure with naturally formed xylem vessels and lumina (channels) in parallel to the membrane surface (Fig. 2D). The channel diameters ranged from 10 to 100 μm, and the channel pores granted the hydrophobic natural wood membrane a porous structure with a porosity of 21 ± 3%. Impressively, the removal of intermixed lignin and hemicellulose contributed to ~70% mass loss in the wood structure and, thus, further improved the porosity more than four times from 21 ± 3 to 89 ± 3% for the hydrophobic nanowood membrane. Note that the porosity of the hydrophobic nanowood membrane was also larger than that of commercial membranes, of which the porosity ranged from 41 to 85% (Table 1) (10, 15, 22, 25, 28). In addition to porosity augmentation, the removal of lignin and hemicellulose greatly shifted the PSD to the right (Fig. 2I) and increased the average pore size by ~56% from 0.18 ± 0.02 to 0.28 ± 0.03 μm (Table 1). We observed the obtained pore structure of the hydrophobic nanowood membrane using SEM (Fig. 2, D to H). Along the cross-sectional direction, we also detected micropores amid the crystalline cellulose nanofibrils (<100 nm; Fig. 2F). Apart from the pores between nanofibrils, we also observed a large amount of mesopores (pits) growing on the xylem vessels and lumina (5 to 10 μm; Fig. 2, E, G, and H), which were used for water and nutrient delivery during tree growth. This study takes advantage of the gas transportation property of these pores located either between the nanofibrils or on the channel walls for water vapor transportation. The unique pore structure of the hydrophobic nanowood membrane resulted in the nonuniform PSD with several peaks, which were totally different from the commercial PP and PTFE membranes with very uniform PSDs (fig. S6). Benefiting from the large porosity, the theoretical thermal conductivity of the hydrophobic nanowood membrane was decreased from 0.210 to 0.040 W m^{-1} K^{-1} at 25°C (section S12), which would contribute to conductive heat loss reduction.
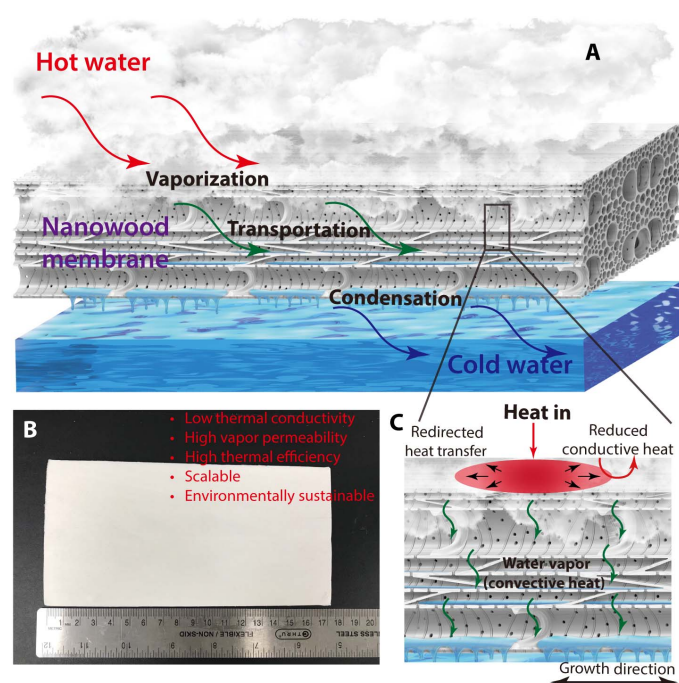

Fig. 1. The process schematic of nanowood membranes for MD. (**A**) Schematic of MD using the wood membrane. (**B**) Digital photograph of the nanowood and the corresponding beneficial properties for MD applications. (**C**) Schematic of the water (vapor) and heat transfer in the wood membrane during MD. Photo credit: T. Li, University of Maryland.
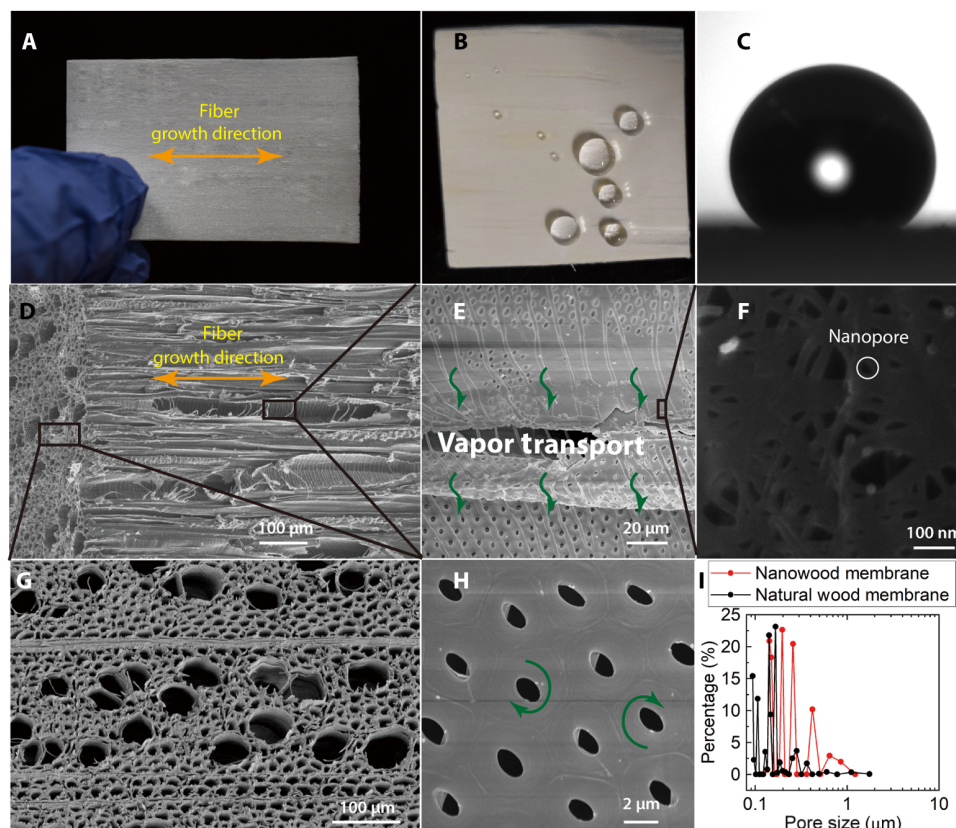
Fig. 2. Structural characterization of the nanowood membrane. (**A**) Photo of the hydrophobic nanowood membrane. (**B**) Photo that shows hydrophobicity after silane treatment. (**C**) Water contact angle of the nanowood membrane. (**D**) SEM images of the nanowood surface that exhibit aligned texture, xylem vessels, and lumina (channels). (**E**) SEM images that exhibit mesopores [(**G**) cross section and (**H**) pits] growing on the walls of the xylem vessels and lumina. (**F**) SEM images that exhibit microsized pores amid the cellulose fibers. (**I**) PSD of the hydrophobic natural wood and nanowood membranes. Photo credit: D. Hou, University of Colorado.

Moreover, different from the commercial membranes with isotropic structures and intertwined fibers (fig. S7), the aligned and high–aspect ratio nanofibril channels led to anisotropic heat flow along the alignment direction rather than the cross-sectional direction, which can further prevent the heat transfer across the wood membrane (*39*). In addition, the increased pore size and porosity were hypothesized to improve vapor permeability and enhance water flux (section 12), thereby increasing convective heat transfer (*10*).

As shown in Fig. 2C and fig. S8, both the hydrophobic nanowood membrane and natural wood membrane had water contact angles greater than 140°, indicating that the initially highly hydrophilic wood substrate (i.e., no measurable water contact angle) was successfully modified to be hydrophobic after surface fluorination. The hydrophobicity of the treated wood membranes was better than those commercial membranes with PTFE or PP substrate, where the contact angles were lower than 130° (Table 1) (*22, 26*). The excellent hydrophobicity of the wood membranes was attributed to fluoroalkylsilane (FAS) treatment, which has super low surface energy (13.1 mN m^{-1}) compared to PTFE (20 mN m^{-1}) and PP (30 mN m^{-1}) (*26, 44*). Note that the surface morphologies and pore structure did not change before and after surface fluorination by FAS (fig. S2). Owing to the good hydrophobicity and relatively small pore size, the nanowood membrane demonstrated decent liquid entry pressure (LEP; ~74.7 ± 0.5 kPa), suggesting a better resistance to membrane wetting than the commercial PP membranes. However, it was noted that the nanowood membrane showed smaller LEP than the PTFE membrane (~130 kPa).

This is due to the wide PSD of the nanowood membrane, as larger pores (>0.4 μm) may exert negative effects (*45*).

Thermal conductivity characterization of the nanowood membrane

To demonstrate the thermal insulation capabilities of the fabricated hydrophobic nanowood membrane, we tested the specimens under a conductive heat source to simulate the DCMD. We measured the temperature with an infrared radiation (IR) camera (Fig. 3). Five different temperatures were applied, and the results show that the hydrophobic nanowood membrane yielded lower backside temperature than the hydrophobic natural wood membrane, attributed to its low thermal conductivity and anisotropic property (*39*).

The thermal conductivity of both nanowood and natural wood increased gradually from 0.210 to 0.270 W m^{-1} K^{-1} and from 0.040 to 0.049 W m^{-1} K^{-1}, respectively, with the escalation of the heat source temperature from 40° to 60°C (Fig. 3E). This is assumed because of the increase in conductivity of the cell wall substances rather than the increase in gas phase conductivity or the radiative conductivity (*46*). The trend was more notable for the natural wood (29%) than for nanowood (23%) due to the presence of hemicellulose and lignin, which are of less thermal stability (*47*). The measured thermal conductivity was comparable to the theoretical values (section S12), which are 0.184 and 0.037 W m^{-1} K^{-1} at 25°C for natural wood and nanowood membranes, respectively. The nanowood membrane showed lower thermal conductivity than most of the commercial membranes, whose
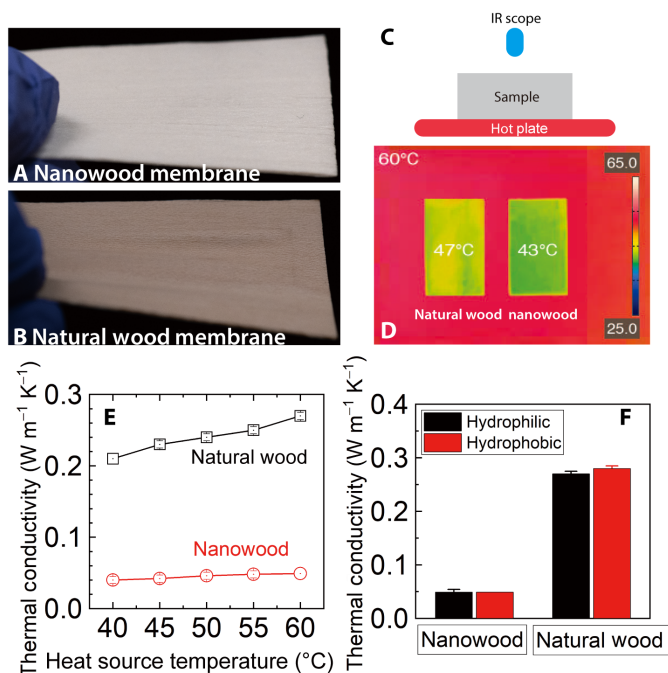
Fig. 3. Thermal conductivity characterization of the wood membranes. (**A**) Photo of the hydrophobic nanowood membrane. (**B**) Photo of the hydrophobic natural wood membrane. (**C**) Schematic representation of contact heat source measurement. IR thermographs of (**D**) the wood membranes. (**E**) Measured thermal conductivity of the wood membranes from 40° to 60°C. (**F**) Comparison of the thermal conductivity of the woods at 60°C before and after hydrophobic silane treatment. Error bars represent the SDs based on three independent experiments. Photo credit: D. Hou, University of Colorado.

thermal conductivity is generally higher than 0.045 W m^{-1} K^{-1}. This lower thermal conductivity was believed to reduce the conductive heat loss during MD and maintain the effective temperature gradient across the membrane. When heated by a conductive heat source at 60°C, it was shown that the stabilized backside temperature of the hydrophobic natural wood was 47°C, whereas that of the hydrophobic nanowood was 43°C, under 200 mW cm^{-2} (Fig. 3D). This directly indicated that the nanowood exhibited better thermal insulation property or less conductive heat loss than the natural wood. Accordingly, the thermal conductivity of the nanowood membrane was 0.049 ± 0.002 W m^{-1} K^{-1} at 60°C (Fig. 3E), which was only 18% of the thermal conductivity of the natural wood membrane (0.270 ± 0.005 W m^{-1} K^{-1} at 60°C). This significantly lower thermal conductivity of nanowood membrane was attributed not only to the higher porosity (89 ± 3% versus 21 ± 3%) but also to bigger pore size (0.28 ± 0.03 μm versus 0.18 ± 0.02 μm). Previous study indicated that higher interspacing (pore size) between fibers than the mean free path of air can mitigate thermal conduction through air. The reduction of microsized and nanosized pores is appreciable for further reduction of thermal conductivity (*39*). Furthermore, hemicellulose (0.34 W m^{-1} K^{-1}) and lignin (0.39 W m^{-1} K^{-1}) carried higher thermal conductivity than the nanocrystalline cellulose (0.26 W m^{-1} K^{-1}). Therefore, the removal of intermixed lignin and hemicellulose greatly reduced the bulk thermal conductivity of nanowood. Note that the hydrophobic treatment with FAS did not result in significant change of the thermal conductivity of the wood (Fig. 3F).

Thermally efficient desalination of the nanowood membrane
Figure 4 shows the water (vapor) flux through the hydrophobic wood membranes. Accompanied by the increase in feed temperature from

Table 1. Characteristic comparisons of the new wood membranes and commercial polymeric membranes. LEP, liquid entry pressure; ECTFE, ethylene chlorotrifluoroethylene.

Membrane	Manufacturer	Active layer	Support material	Pore size (μm)	Thickness (μm)	Porosity (%)	Contact angle (°)	LEP (kPa)	Intrinsic permeability (×10^{-10} kg m^{-1} s^{-1} Pa^{-1})	Thermal conductivity (W m^{-1} K^{-1})*	Thermal efficiency (%)[†]	Reference
ECTFE	3M	ECTFE	–	0.43[‡]	46	67	118	–	0.39	~0.034	~60	(*22*)
0.45PP	3M	PP	–	0.79[‡]	110	85	130	–	0.95	0.048	~58	(*22*)
QM902	Clarcor	ePTFE	–	0.45[‡]	–	70-85	–	–	–	–	~51	(*22*)
2400	Celgard	PP	–	0.043[‡]	25	41	138	–	0.02	0.111	<3	(*22*)
0.22PP	Tisch	PP	–	1.79 ± 0.10[§]	196 ± 18	72 ± 3	119	42.7 ± 0.3	0.64 ± 0.02	0.066	44 ± 1	This study
0.45PP	Tisch	PP	–	2.65 ± 0.24[§]	175 ± 4	72 ± 1	125	38.6 ± 0.5	0.68 ± 0.04	0.066	39 ± 3	This study
0.22PTFE	Tisch	PTFE	PP	0.33 ± 0.00[§]	188 ± 5	75 ± 4	121	126 ± 2	1.21 ± 0.22	0.082	53 ± 0	This study
0.45 PTFE	Tisch	PTFE	PP	0.36 ± 0.00[§]	156 ± 11	78 ± 2	117	133 ± 5	1.15 ± 0.21	0.075	59 ± 2	This study
Natural wood		Cellulose	–	0.18 ± 0.02[§]	540 ± 15	21 ± 3	142	98.5 ± 0.8	0.20 ± 0.04	0.210	12 ± 2	This study
Nanowood		Cellulose	–	0.28 ± 0.03[§]	502 ± 35	89 ± 3	144	74.7 ± 0.5	1.44 ± 0.09	0.040[‖]	71 ± 2	This study

*The theoretical values were based on the assumption of isotropic thermal property (in this table and section S12) (*39, 47, 59*). However, the real nanowood is anisotropic with a measured, while the anisotropic thermal conductivity in *x* (fiber growth direction), *y*, and *z* (transverse direction) directions was 0.060, 0.030, and 0.030 W m^{-1} K^{-1}, respectively. †The experimental feed temperature and distillate temperature were 60° and 20°C, respectively. ‡Nominal pore size. §Averaged pore size. ‖Theoretical thermal conductivity at room temperature.

40° to 60°C, water flux through the hydrophobic natural wood and nanowood membranes raised from 1.4 ± 0.2 to 3.4 ± 0.5 kg m^{-2} hour^{-1} and from 5.1 ± 0.1 to 20.8 ± 0.8 kg m^{-2} hour^{-1}, respectively. Although the hydrophobic nanowood membrane was comparable in thickness to the hydrophobic natural wood membrane, it demonstrated up to ~6.1 times higher water flux, owing to the increase in porosity (4.2 times) and pore size (1.6 times), which substantially reduced the vapor transfer resistance. At feed and distillate temperatures of 60° and 20°C, respectively, the water flux through the hydrophobic nanowood membrane (20.8 ± 0.8 kg m^{-2} hour^{-1}) was close to that of the commercial PP membranes (~22.5 kg m^{-2} hour^{-1}) (Fig. 4A and fig. S10). The comparable flux was attributed to the much higher porosity (89 ± 3%) over the PP (~72%) membrane, which compensated for the disadvantage of higher thickness (502 ± 35 μm versus ~180 μm). It was not unusual that all the PTFE membranes exhibited far better water flux (up to 54.2 ± 3.1 kg m^{-2} hour^{-1} for 0.45 PTFE at 60°C) than the wood membranes. The better water flux should be attributed to the much smaller thickness (~130 μm versus ~500 μm of nanowood membrane), which greatly reduced the vapor transfer resistance. However, when normalized by thickness, the nanowood membrane demonstrated a very high intrinsic permeability (1.44 ± 0.09 kg m^{-1} K^{-1} s^{-1} Pa^{-1}), which was ~2 times and ~1.2 times better than that of the PP (~0.65 kg m^{-1} K^{-1} s^{-1} Pa^{-1}) and PTFE (~1.2 kg m^{-1} K^{-1} s^{-1} Pa^{-1}) membranes, respectively (Fig. 4C). The higher permeability was attributed to the much higher porosity (89 ± 3%) over the PP (~72%) and PTFE (~75%) membranes. The experimental permeability was supported by the theoretical values based on the dusty gas model, which indicated that the vapor permeation through the wood and PTFE membranes with smaller pore sizes (<1.4 μm; 100 times the mean free path of water vapor at 50°C) was dominated by the Knudsen and ordinary molecular diffusion (48, 49). This was different from the PP membrane (pore size, >1.7 μm) with viscous diffusion as the primary transport mechanism. In concordance with the results of other studies, the intrinsic permeability of both the nanowood and commercial membranes was generally higher than the theoretical permeability (fig. S13), which assumed cylindrical nonconnected pores with uniform size (section S15) (23, 24). It was hypothesized that the enhanced ordinary molecular diffusion through the large pores amid cellulose fibers and viscous diffusion in the interconnected nanowood channels attributed to the 26% higher intrinsic permeability compared to that of the PTFE membranes (23, 24). Another contributing factor might be the anisotropic thermal property of the nanowood membrane (section S5), which was believed to facilitate heat transfer along the membrane, thereby helping maintain the temperature gradient and promote flux. Although the nanowood demonstrated ~20% higher porosity and intrinsic permeability, the advantages were offset by disadvantages of its higher thickness and smaller pore size (0.28 ± 0.03 μm versus ~0.34 μm of PTFE membranes) (10). Therefore, thinner wood membranes should be fabricated for better flux in future studies (10). Figure S16 shows the water flux of wood membrane (salt rejection, >99.8%) kept stable for at least 6 hours before declining because of wetting. However, the performance recovered after deionized (DI) water and ethanol rinsing, followed by drying. Improved silane treatment such as adding silica nanoparticles may help extend the membrane's longevity without changing the wood structure (44, 50).

The thermal efficiency is a performance parameter in determining the energy efficiency (10, 22). Thermal efficiency can indicate how effectively the membrane uses thermal gradient for vapor transfer as compared to conductive heat loss (22). A higher thermal efficiency results from higher convective heat transfer and/or less conductive heat transfer through the membrane material (10). For the membranes in the study, the thermal efficiency has a substantial dependence on water flux (feed temperature; Fig. 4D). The thermal efficiency of both nanowood and natural wood membranes increased along with the heat source temperature increased from 40° to 60°C. This is believed to be associated with the faster evolution of convective heat transfer than conductive heat transfer. Moreover, the hydrophobic nanowood membrane demonstrated a good thermal efficiency of up to 71 ± 2% at 60°C, representing one of the highest values achieved in MD so far (22). In contrast, the hydrophobic natural wood membrane had a very limited thermal efficiency of 12 ± 2%. As a result, this membrane would require six times more energy for operation compared to the hydrophobic nanowood membrane. The good thermal efficiency of the hydrophobic nanowood membrane was ascribed not only to its super low thermal conductivity (0.080 versus 0.30 ± 0.02 W m^{-1} K^{-1} for natural wood membrane at 60°C) but also to its high porosity (89 ± 3% versus 21 ± 3%) and bigger pore size (0.28 ± 0.03 μm versus 0.18 ± 0.02 μm). The low membrane thermal conductivity reduced the conductive heat transfer through a membrane material, while the high porosity and bigger pore size reduced water transfer resistance, thereby enhancing water flux and convective heat transfer (10, 21, 22). The superior thermal insulation property prevented conductive heat loss and offset the limitation of low water flux and convective heat transfer. Benefiting from low thickness and higher porosity, the commercial 0.45 PTFE membrane exhibited the highest water flux among all membranes tested. However, note that the 0.45 PTFE membrane demonstrated a lower intrinsic permeability (1.15 ± 0.16 × 10^{-10} kg m^{-1} s^{-1} Pa^{-1}) than
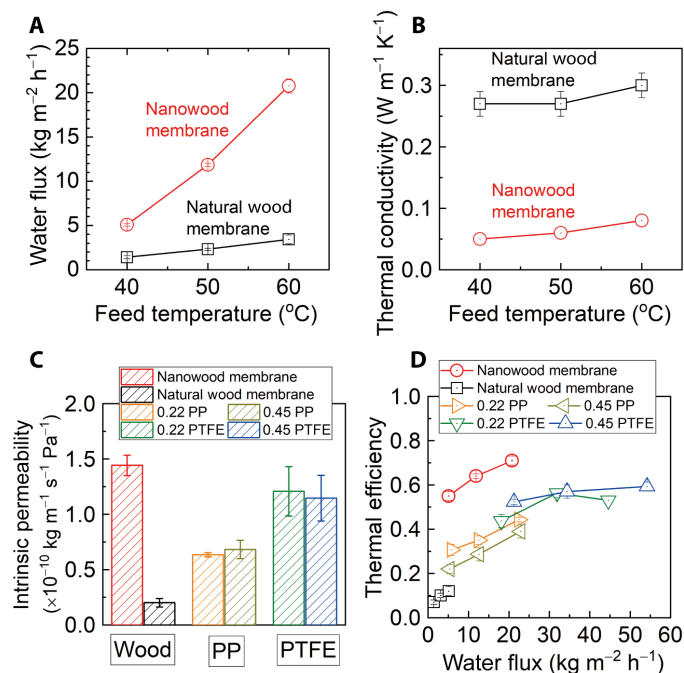

Fig. 4. MD performance of the wood and commercial membranes. (**A**) Water flux and (**B**) experimental thermal conductivities for the hydrophobic wood membranes with feed temperature continuously varying between 40° and 60°C and distillate temperature of 20°C. (**C**) Intrinsic permeability of the membranes. (**D**) Thermal efficiency versus water flux of the wood membranes and commercial membranes. Error bars represent the SDs based on three independent experiments.

that of the nanowood membrane ($1.44 \pm 0.09 \times 10^{-10}$ kg m^{-1} s^{-1} Pa^{-1}) at 60°C, indicating comparatively limited convective heat transfer (24). In addition, suffering from higher thermal conductivity and, thereby, higher conductive heat transfer, its thermal efficiency (59 ± 2%) was lower than that of the nanowood membrane, meaning that the nanowood membrane produced 1.2 times the freshwater permeate of the commercial PTFE membranes per kilojoule of heat energy at 60°C. Although the commercial PP membranes show smaller thermal conductivity than the PTFE membranes, the limited intrinsic permeability ($\sim 0.65 \times 10^{-10}$ kg m^{-1} s^{-1} Pa^{-1}) restricted the convective heat flux and, thus, resulted in low thermal efficiency (up to 44 ± 1% for 0.22PP; Table 1) at 60°C. The intrinsic permeability of nanowood in this study was comparable to that of a fibrous cellulose aerogel membrane ($\sim 1.4 \times 10^{-10}$ kg m^{-1} s^{-1} Pa^{-1}) with a high porosity of 98% (24). This suggests that owing to a unique structure with larger pore size and wider PSD, the nanowood membrane offsets the disadvantage from lower porosity (23). However, note that the effect of the unique anisotropic structure with large PSD on the heat and mass transfer is still unclear and requires further investigation.

IMPLICATIONS AND FUTURE WORK

Completely derived from abundant and sustainable natural wood, the newly developed hydrophobic nanowood membrane demonstrated superior properties and potential in MD for water desalination. The membrane exhibited good water flux (water vapor transportation) and excellent thermal efficiency (up to 70%), comparable or even higher than commercial polymeric membranes that are made of petroleum products. The exceptional thermal efficiency was attributed to its high intrinsic permeability (1.44 ± 0.09 kg m^{-1} K^{-1} s^{-1} Pa^{-1}) and super low thermal conductivity (0.040 W m^{-1} K^{-1}), which promoted convective and conductive heat transfer, respectively. In addition, the anisotropic thermal property of the nanowood membrane was believed to facilitate the heat transfer along the membrane, thereby helping to maintain the temperature gradient and promote flux. However, to quantify these benefits, localized temperature differences will need to be measured and compared. Instead of using complex fabrication processes such as those for PP and PTFE manufacturing, the nanowood membrane can be fabricated by a scalable top-down approach via simple chemical treatments. As a proof of concept for scalability, we have constructed pieces of the nanowood membrane with a length larger than 15 cm and a thickness less than 500 μm. The newly developed nanowood membrane as a thermally efficient membrane carries great potential to use low-grade heat from different sources for water desalination. Optimizations of the pore size and thickness can be achieved by selecting other wood species and using microtomes. Future bio-based wood membrane with this unique pore structure may also be engineered using nanocellulose fibers via electrospinning. Because of the hydrophilic nature of nanocellulose materials, further improvements are needed to increase hydrophobic treatment efficacy and membrane durability under high temperature and chemical conditions. In addition, fabrication methods need to be improved to generate thinner and larger membrane materials.

MATERIALS AND METHODS
Materials and chemicals
All working solutions were prepared using American Chemical Society–grade chemicals (Thermo Fisher Scientific, Waltham, MA) and Milli-Q water (18.2 megohm·cm) throughout the study, unless otherwise stated.

The lignin removal solution contained 2.5 M NaOH and 0.4 M Na$_2$SO$_3$, and the bleaching solution was 2.5 M H$_2$O$_2$. A mixture of 95 weight % (wt %) ethanol, 2 wt % FAS (perfluorodecyltriethoxysilane, C$_{16}$H$_{19}$F$_{17}$O$_3$Si; Sigma-Aldrich), and 3 wt % Milli-Q water (pH adjusted at pH 5.0 with acetic acid) was prepared and used as the silane solution for hydrophobic treatment. The mixture was magnetically stirred for 24 hours for silane hydrolysis. The mechanism of silane treatment can be found in section S1 (50). Commercial hydrophobic membranes (Table 1 and fig. S5) in comparison tests were purchased from Tisch Scientific, North Bend, OH.

Nanowood membrane preparation and characterization
The base wood used in this study was American basswood purchased from Walnut Hollow Company. Two types of woods were prepared for membrane fabrication. One type of membrane was made from natural wood without lignin treatment, and another was constructed using treated nanowood, which underwent lignin removal process to increase flexibility and porosity. The nanowood was prepared from natural wood slices (thickness, 2 mm) by boiling the wood along cellulose fiber direction for 12 hours, followed by rinsing in hot distilled water three times to remove residuals (51, 52). The product was subsequently immersed in the boiling bleaching solution until the wood turned white (Fig. 3, A and B). Last, each wood sample was rinsed with cold water and freeze-dried to preserve the nanoporous structure of the delignified wood (39).

Similar procedures were used on pieces of nanowood and natural wood for membrane fabrication. After the above treatment, the average thickness of the nanowood was 502 ± 35 μm, while the average thickness of natural wood was 540 ± 15 μm (fig. S3). Wood consists of naturally aligned cellulose fibers with abundant hydroxyl functional groups that allow surface modification via silane chemistry (fig. S1). The nanowood was dipped into the FAS solution with gentle agitation for 10 hours to enable full infiltration before thorough ethanol rinse. Then, the FAS-treated wood was subjected to heat treatment at 120°C for 4 hours in a vacuum oven (−80 kPa). After this treatment, the hydrophilic wood membranes became hydrophobic with FAS loadings of wood (71.3 ± 5.4 mg FAS g^{-1}). The membrane samples were characterized using SEM, contact angle measurements, PSD, porosity, and thermal conductivity (24, 39, 53–55), and the performance in desalination was compared with commercial MD membranes.

Contact angle and LEP measurements
Contact angle measurements were performed using a contact angle goniometer (Model 250, ramé-hart, Netcong, NJ) via sessile drop method (54). The measurements were performed by placing the sample on the measurement platform coupled with a camera lens to capture the image. A 3-μl DI water droplet was deposited by a syringe placed above the surface. The contact angle was measured and analyzed using the built-in software. At least three measurements were conducted on each of the three different locations for one membrane sample, and the data were averaged.

The LEP was measured using a stainless membrane cell (Sartorius), where DI water was placed on the membrane and the pressure in the sample holder was increased by flowing nitrogen gas. The pressure at which the gas flow was detected by a flow meter was reported as the LEP.

PSD and porosity measurements
The PSD of the prepared membranes was determined using a capillary flow porometer (CFP; Porolux 1000, IB-FT GmbH, Germany). The

membrane was fully wetted with Porefil, followed by measurements described by Nakao (53) and Khayet and Matsuura (56). The PSD was obtained with the aid of the coupled CFP software.

Membrane porosity was determined using the gravimetric method (24, 55). Specifically, a piece of membrane was dried at 40°C for 5 hours in an oven and subsequently weighed using an analytical balance (Denver PI-214A). The sample was then fully immersed into 2-propanol for 1 day for complete alcohol infiltration. After wetting, the sample was cleaned to remove residue from the surface and weighed. The porosity (ε) was estimated using the equation

$$\varepsilon = \frac{V_{\text{pore}}}{V_{\text{total}}} = \frac{m_{\text{IPA}} / \rho_{\text{IPA}}}{V_{\text{total}}} \qquad (1)$$

where V, m, and ρ are the volume, mass, and density, respectively, and IPA indicates 2-propanol. Three independent measurements were performed on each sample.

Thermal property measurements

The thermal properties of the membranes were characterized using a conductive heat source with a contact area of 4 mm by 4 mm via conductive thermal paste. IR thermographs were taken using an IR camera (T630sc from FLIR). Steady state was reached before the data were recorded at room temperature (21°C). The thermal conductivity of woods was measured using the laser flash apparatus (LFA), during which an instantaneous laser pulse was used to heat up one side of the sample, and the response of temperature on the other side was recorded by a detector. The thermal conductivity κ of the sample was calculated according to Li et al. (39). Briefly, an instantaneous laser pulse was irradiated on one side of the sample, and the response of temperature on the other side was recorded by an LFA 457 detector (NETZSCH, Burlington, MA) for thermal diffusivity measurement. Differential scanning calorimetry method with a sapphire reference was used to determine the heat capacity. The thermal conductivity k can then be calculated by multiplying the thermal diffusivity and the heat capacity together with the material bulk density (0.13 ± 0.03 g cm^{-3}). The samples were stored at 25°C and 20% humidity for a minimum of 24 hours before measurement.

MD reactor and operation

Membrane performance was evaluated using a laboratory-scale DCMD apparatus (fig. S9). The membranes were inserted into the custom-built acryl cell with an effective membrane area of 8 cm^2 (4-cm length by 2-cm width). Hot feed [NaCl (1 g liter^{-1})] and cold distillate (DI) streams were circulated using two variable gear pumps (Cole-Parmer, Vernon Hills, IL), and temperature was controlled using two recirculating water baths (Polystat Standard, Cole-Parmer, Vernon Hills, IL). Diamond-shaped polyester spacers were inserted in both feed and distillate channels to support and maintain membrane geometry in the cell. During operation, cocurrent flow, which was parallel to the fiber growth direction of the wood membrane, was adopted with a flow rate of 220 ml min^{-1} (equivalent to a cross flow velocity of 8.0 cm s^{-1}) for both feed and distillate. Water vapor flux, J_w, across the membrane was measured by monitoring the increase in distillate mass using a digital balance (NVT6200, OHAUS, Parsippany, NJ). The distillate weight gain was recorded in a laptop at 1-min intervals. Salt passage was monitored by measuring the salt concentration in distillate using a calibrated conductivity meter (OAKTON Instruments, Vernon Hills, IL) at 1-min

intervals. Membrane performance for every sample was measured for three different sets of feed temperatures (40°, 50°, and 60°C), while the distillate temperature was fixed at 20°C. Each temperature set was operated for 30 min. The experimental thermal conductivity and intrinsic permeability were calculated according to a modified Schofield method (section S14) (22). The transport mechanism and theoretical permeability of water vapor through the membrane (section S15) were simulated using the widely adopted "dusty gas model," which considered viscous diffusion, ordinary molecular diffusion, and Knudsen diffusion (23, 24, 57, 58).

SUPPLEMENTARY MATERIALS

Supplementary material for this article is available at http://advances.sciencemag.org/cgi/content/full/5/8/eaaw3203/DC1

Section S1. The hydrophobic silane treatment mechanism
Section S2. The nanowood membrane before and after hydrophobic treatment
Section S3. The natural wood membranes
Section S4. Comparison of the wood membranes and common papers
Section S5. Anisotropic thermal insulation property of the nanowood membrane and the potential benefits
Section S6. Commercial hydrophobic membranes
Section S7. Pore size distribution of the commercial membranes
Section S8. Morphology and pore structure of the commercial membranes
Section S9. Surface hydrophobicity/hydrophilicity
Section S10. DCMD reactors and configurations
Section S11. Water flux of commercial membranes
Section S12. Theoretical thermal conductivity estimation
Section S13. Thermal insulation of commercial membranes
Section S14. Experimental thermal conductivity and membrane permeability
Section S15. Theoretical permeability coefficient and intrinsic permeability
Section S16. Wood membrane durability
Section S17. Wood membrane application and fouling
Fig. S1. Schematics of hydrophobic treatment of wood membranes using silane coupling agent (50).
Fig. S2. Surface morphologies and pore size distribution of the nanowood membrane before and after hydrophobic treatment.
Fig. S3. Visual images of the hydrophobic natural wood membrane after silane treatment.
Fig. S4. Temperature plots of isotropic and anisotropic thermal insulators from a point heat source.
Fig. S5. Visual images of the commercial hydrophobic membranes purchased from Tisch Scientific (North Bend, Ohio).
Fig. S6. PSD of the commercial membranes.
Fig. S7. SEM images of the surface and cross-section of the commercial membranes.
Fig. S8. Water contact angles of the commercial and hydrophobic natural wood membranes.
Fig. S9. Schematics, images, and control interface of the apparatus for direct contact membrane distillation (DCMD).
Fig. S10. Water flux of the commercial polymeric membranes in DCMD with feed [NaCl (1 g liter^{-1})] temperature continuously varying between 40° and 60°C and distillate (DI water) temperature of 20°C.
Fig. S11. IR thermographs of the commercial membranes with the heat source temperature of 60°C.
Fig. S12. Temperature plots of anisotropic nanowood and isotropic commercial membranes from a point heat source.
Fig. S13. Comparison of experimentally measured intrinsic (thickness-normalized) membrane permeability of the wood and commercial membranes.
Fig. S14. Water flux of the hydrophobic wood membranes in DCMD with feed [NaCl (1 g liter^{-1})] and distillate (DI water) temperatures controlled at 60° and 20°C, respectively.
Fig. S15. Water flux of the hydrophobic nanowood membrane in DCMD with [NaCl (35 g liter^{-1}) and synthetic wastewater] and distillate (DI water) temperatures controlled at 60° and 20°C, respectively.
Table S1. Comparison between nanowood and common paper.

REFERENCES AND NOTES

1. United Nations World Water Assessment Programme, "The United Nations world water development report 2018: Nature-based solutions for water" (United Nations Educational, Scientific and Cultural Organization, 2018).

2. G. M. MacDonald, Climate change and water in southwestern North America special feature: Water, climate change, and sustainability in the southwest. *Proc. Natl. Acad. Sci. U.S.A.* **107**, 21256–21262 (2010).

3. W. N. Adger, J. Barnett, K. Brown, N. Marshall, K. O'Brien, Cultural dimensions of climate change impacts and adaptation. *Nat. Clim. Chang.* **3**, 112–117 (2012).

4. A. AghaKouchak, D. Feldman, M. Hoerling, T. Huxman, J. Lund, Water and climate: Recognize anthropogenic drought. *Nature* **524**, 409–411 (2015).

5. M. A. Shannon, P. W. Bohn, M. Elimelech, J. G. Georgiadis, B. J. Mariñas, A. M. Mayes, Science and technology for water purification in the coming decades. *Nature* **452**, 301–310 (2008).

6. M. Elimelech, W. A. Phillip, The future of seawater desalination: Energy, technology, and the environment. *Science* **333**, 712–717 (2011).

7. C. Forrestal, Z. Stoll, P. Xu, Z. J. Ren, Microbial capacitive desalination for integrated organic matter and salt removal and energy production from unconventional natural gas produced water. *Environ. Sci. Water Res. Technol.* **1**, 47 (2015).

8. D. Jassby, T. Y. Cath, H. Buisson, The role of nanotechnology in industrial water treatment. *Nat. Nanotechnol.* **13**, 670–672 (2018).

9. A. Al-Karaghouli, L. L. Kazmerski, Energy consumption and water production cost of conventional and renewable-energy-powered desalination processes. *Renew. Sustain. Energy Rev.* **24**, 343–356 (2013).

10. A. Deshmukh, C. Boo, V. Karanikola, S. Lin, A. P. Straub, T. Tong, D. M. Warsinger, M. Elimelech, Membrane distillation at the water-energy nexus: Limits, opportunities, and challenges. *Energ. Environ. Sci.* **11**, 1177–1196 (2018).

11. P. Denholm, M. O'Connell, G. Brinkman, J. Jorgenson, *Overgeneration from Solar Energy in California. A Field Guide to the Duck Chart* (National Renewable Energy Laboratory, 2015).

12. A. V. Dudchenko, C. Chen, A. Cardenas, J. Rolf, D. Jassby, Frequency-dependent stability of CNT Joule heaters in ionizable media and desalination processes. *Nat. Nanotechnol.* **12**, 557–563 (2017).

13. P. Tao, G. Ni, C. Song, W. Shang, J. Wu, J. Zhu, G. Chen, T. Deng, Solar-driven interfacial evaporation. *Nat. Energy* **3**, 1031–1041 (2018).

14. A. Alkhudhiri, N. Darwish, N. Hilal, Membrane distillation: A comprehensive review. *Desalination* **287**, 2–18 (2012).

15. B. L. Pangarkar, M. G. Sane, S. B. Parjane, M. Guddad, Status of membrane distillation for water and wastewater treatment—A review. *Desalin. Water Treat.* **52**, 5199 (2013).

16. E. Drioli, A. Ali, F. Macedonio, Membrane distillation: Recent developments and perspectives. *Desalination* **356**, 56–84 (2015).

17. A. P. Straub, N. Y. Yip, S. Lin, J. Lee, M. Elimelech, Harvesting low-grade heat energy using thermo-osmotic vapour transport through nanoporous membranes. *Nat. Energy* **1**, 16090 (2016).

18. P. D. Dongare, A. Alabastri, S. Pedersen, K. R. Zodrow, N. J. Hogan, O. Neumann, J. Wu, T. Wang, A. Deshmukh, M. Elimelech, Q. Li, P. Nordlander, N. J. Halas, Nanophotonics-enabled solar membrane distillation for off-grid water purification. *Proc. Natl. Acad. Sci. U.S.A.* **114**, 6936–6941 (2017).

19. P. Zhang, J. Li, L. Lv, Y. Zhao, L. Qu, Vertically aligned graphene sheets membrane for highly efficient solar thermal generation of clean water. *ACS Nano* **11**, 5087–5093 (2017).

20. M. Qtaishat, T. Matsuura, B. Kruczek, M. Khayet, Heat and mass transfer analysis in direct contact membrane distillation. *Desalination* **219**, 272–292 (2008).

21. A. Deshmukh, M. Elimelech, Understanding the impact of membrane properties and transport phenomena on the energetic performance of membrane distillation desalination. *J. Memb. Sci.* **539**, 458–474 (2017).

22. J. Vanneste, J. A. Bush, K. L. Hickenbottom, C. A. Marks, D. Jassby, C. S. Turchi, T. Y. Cath, Novel thermal efficiency-based model for determination of thermal conductivity of membrane distillation membranes. *J. Memb. Sci.* **548**, 298–308 (2018).

23. M. Khayet, Membranes and theoretical modeling of membrane distillation: A review. *Adv. Colloid Interface Sci.* **164**, 56–88 (2011).

24. M. E. Leitch, C. Li, O. Ikkala, M. S. Mauter, G. V. Lowry, Bacterial nanocellulose aerogel membranes: Novel high-porosity materials for membrane distillation. *Environ. Sci. Technol. Lett.* **3**, 85–91 (2016).

25. A. M. Alklaibi, N. Lior, Membrane-distillation desalination: Status and potential. *Desalination* **171**, 111–131 (2005).

26. P. Wang, T.-S. Chung, Recent advances in membrane distillation processes: Membrane development, configuration design and application exploring. *J. Memb. Sci.* **474**, 39–56 (2015).

27. D. Hou, A. Iddya, X. Chen, M. Wang, W. Zhang, Y. Ding, D. Jassby, Z. J. Ren, Nickel-based membrane electrodes enable high-rate electrochemical ammonia recovery. *Environ. Sci. Technol.* **52**, 8930–8938 (2018).

28. M. Gryta, Osmotic MD and other membrane distillation variants. *J. Memb. Sci.* **246**, 145–156 (2005).

29. T. Borca-Tasciuc, S. Vafaei, D.-A. Borca-Tasciuc, B. Wei, R. Vajtai, P. Ajayan, Anisotropic thermal diffusivity of aligned multiwall carbon nanotube arrays. *J. Appl. Phys.* **98**, 054309 (2005).

30. L. Guo, J. Wang, Z. Lin, S. Gacek, X. Wang, Anisotropic thermal transport in highly ordered TiO2 nanotube arrays. *J. Appl. Phys.* **106**, 123526 (2009).

31. B. Wicklein, A. Kocjan, G. Salazar-Alvarez, F. Carosio, G. Camino, M. Antonietti, L. Bergstrom, Thermally insulating and fire-retardant lightweight anisotropic foams based on nanocellulose and graphene oxide. *Nat. Nanotechnol.* **10**, 277–283 (2015).

32. N. Lucas, C. Bienaime, C. Belloy, M. Queneudec, F. Silvestre, J. E. Nava-Saucedo, Polymer biodegradation: Mechanisms and estimation techniques. *Chemosphere* **73**, 429–442 (2008).

33. Y. Habibi, L. A. Lucia, O. J. Rojas, Cellulose nanocrystals: Chemistry, self-assembly, and applications. *Chem. Rev.* **110**, 3479–3500 (2010).

34. L. Hu, G. Zheng, J. Yao, N. Liu, B. Weil, M. Eskilsson, E. Karabulut, Z. Ruan, S. Fan, J. T. Bloking, M. D. McGehee, L. Wågberg, Y. Cui, Transparent and conductive paper from nanocellulose fibers. *Energ. Environ. Sci.* **6**, 513–518 (2013).

35. L.-F. Chen, Z.-H. Huang, H.-W. Liang, W.-T. Yao, Z.-Y. Yu, S.-H. Yu, Flexible all-solid-state high-power supercapacitor fabricated with nitrogen-doped carbon nanofiber electrode material derived from bacterial cellulose. *Energ. Environ. Sci.* **6**, 3331–3338 (2013).

36. Y. H. Jung, T.-H. Chang, H. Zhang, C. Yao, Q. Zheng, V. W. Yang, H. Mi, M. Kim, S. J. Cho, D. W. Park, H. Jiang, J. Lee, Y. Qiu, W. Zhou, Z. Cai, S. Gong, Z. Ma, High-performance green flexible electronics based on biodegradable cellulose nanofibril paper. *Nat. Commun.* **6**, 7170 (2015).

37. F. Chen, A. S. Gong, M. Zhu, G. Chen, S. D. Lacey, F. Jiang, Y. Li, Y. Wang, J. Dai, Y. Yao, J. Song, B. Liu, K. Fu, S. Das, L. Hu, Mesoporous, three-dimensional wood membrane decorated with nanoparticles for highly efficient water treatment. *ACS Nano* **11**, 4275–4282 (2017).

38. Z. Huang, A. Gong, A. Dou, L. Hu, Z. J. Ren, A conductive wood membrane anode improves effluent quality of microbial fuel cells. *Environ. Sci. Water Res. Technol.* **3**, 940–946 (2017).

39. T. Li, J. Song, X. Zhao, Z. Yang, G. Pastel, S. Xu, C. Jia, J. Dai, C. Chen, A. Gong, F. Jiang, Y. Yao, T. Fan, B. Yang, L. Wagberg, R. Yang, L. Hu, Anisotropic, lightweight, strong, and super thermally insulating nanowood with naturally aligned nanocellulose. *Sci. Adv.* **4**, eaar3724 (2018).

40. S. A. Lavrykov, B. V. Ramarao, Thermal properties of copy paper sheets. *Drying Technol.* **30**, 297–311 (2012).

41. PaperOnWeb, "Properties of paper"; https://paperonweb.com/paperpro.htm.

42. R. H. White, Effect of lignin content and extractives on the higher heating value of wood. *Wood Fiber Sci.* **19**, 446 (1987).

43. P. T. Larsson, E. L. Hult, K. Wickholm, E. Pettersson, T. Iversen, CP/MAS 13C-NMR spectroscopy applied to structure and interaction studies on cellulose I. *Solid State Nucl. Magn. Reson.* **15**, 31–40 (1999).

44. C. Boo, J. Lee, M. Elimelech, Engineering surface energy and nanostructure of microporous films for expanded membrane distillation applications. *Environ. Sci. Technol.* **50**, 8112–8119 (2016).

45. A. Franken, J. Nolten, M. Mulder, D. Bargeman, C. A. Smolders, Wetting criteria for the applicability of membrane distillation. *J. Memb. Sci.* **33**, 315–328 (1987).

46. B. M. Suleiman, J. Larfeldt, B. Leckner, M. Gustavsson, Thermal conductivity and diffusivity of wood. *Wood Sci. Technol.* **33**, 465–473 (1999).

47. J. Eitelberger, K. Hofstetter, Prediction of transport properties of wood below the fiber saturation point—A multiscale homogenization approach and its experimental validation: Part I. Thermal conductivity. *Compos. Sci. Technol.* **71**, 134–144 (2011).

48. K. W. Lawson, D. R. Lloyd, Membrane distillation. *J. Memb. Sci.* **124**, 1–25 (1997).

49. R. W. Field, H. Y. Wu, J. J. Wu, Multiscale modeling of membrane distillation: Some theoretical considerations. *Ind. Eng. Chem. Res.* **52**, 8822–8828 (2013).

50. S. Lin, S. Nejati, C. Boo, Y. Hu, C. O. Osuji, M. Elimelech, Omniphobic membrane for robust membrane distillation. *Environ. Sci. Technol. Lett.* **1**, 443–447 (2014).

51. M. Zhu, J. Song, T. Li, A. Gong, Y. Wang, J. Dai, Y. Yao, W. Luo, D. Henderson, L. Hu, Highly anisotropic, highly transparent wood composites. *Adv. Mater.* **28**, 5181–5187 (2016).

52. T. Li, M. Zhu, Z. Yang, J. Song, J. Dai, Y. Yao, W. Luo, G. Pastel, B. Yang, L. Hu, Wood composite as an energy efficient building material: Guided sunlight transmittance and effective thermal insulation. *Adv. Energy Mater.* **6**, 1601122 (2016).

53. S.-i. Nakao, Determination of pore size and pore size distribution. *J. Memb. Sci.* **96**, 131–165 (1994).

54. Y. Yuan, T. R. Lee, Contact angle and wetting properties, in *Surface Science Techniques*, G. Bracco, B. Holst, Eds. (Springer, 2013), pp. 3–34.

55. E. Shaulsky, S. Nejati, C. Boo, F. Perreault, C. O. Osuji, M. Elimelech, Post-fabrication modification of electrospun nanofiber mats with polymer coating for membrane distillation applications. *J. Memb. Sci.* **530**, 158–165 (2017).

56. M. Khayet, T. Matsuura, Preparation and characterization of polyvinylidene fluoride membranes for membrane distillation. *Ind. Eng. Chem. Res.* **40**, 5710–5718 (2001).

57. E. A. Mason, A. P. Malinauskas, *Gas Transport in Porous Media: The Dusty-Gas Model*, vol. 17 of *Chemical Engineering Monographs*, A. P. Malinauskas, Ed. (Elsevier, 1983).

58. J. Phattaranawik, R. Jiraratananon, A. G. Fane, Effect of pore size distribution and air flux on mass transport in direct contact membrane distillation. *J. Memb. Sci.* **215**, 75–85 (2003).

59. M. G. Kaganer, *Thermal Insulation in Cryogenic Engineering* (Israel Program for Scientific Translations, 1969).

Citation: D. Hou, T. Li, X. Chen, S. He, J. Dai, S. A. Mofid, D. Hou, A. Iddya, D. Jassby, R. Yang, L. Hu, Z. J. Ren, Hydrophobic nanostructured wood membrane for thermally efficient distillation. *Sci. Adv.* **5**, eaaw3203 (2019).

Science Advances

Hydrophobic nanostructured wood membrane for thermally efficient distillation

Dianxun Hou, Tian Li, Xi Chen, Shuaiming He, Jiaqi Dai, Sohrab A. Mofid, Deyin Hou, Arpita Iddya, David Jassby, Ronggui Yang, Liangbing Hu, and Zhiyong Jason Ren

View the article online
https://www.science.org/doi/10.1126/sciadv.aaw3203
Permissions
https://www.science.org/help/reprints-and-permissions

Use of this article is subject to the Terms of service